Nano Research
DOI 10.1007/s12274-013-0388-5
Research Article
ISSN 1998-0124
CN 11-5974/O4

Carbon nanotube–polypyrrole core–shell sponge and its application as highly compressible supercapacitor electrode

Peixu Li[1], Enzheng Shi[2], Yanbing Yang[3], Yuanyuan Shang[2], Qingyu Peng[2], Shiting Wu[2], Jinquan Wei[4], Kunlin Wang[4], Hongwei Zhu[4], Quan Yuan[3], Anyuan Cao[2] (✉), and Dehai Wu[1] (✉)

[1] *Department of Mechanical Engineering, Tsinghua University, Beijing 100084, China*
[2] *Department of Materials Science and Engineering, College of Engineering, Peking University, Beijing 100871, China*
[3] *Key Laboratory of Analytical Chemistry for Biology and Medicine (Ministry of Education), College of Chemistry and Molecular Sciences, Wuhan University, Wuhan 430072, China*
[4] *Key Laboratory for Advanced Materials Processing Technology and School of Materials Science and Engineering, Tsinghua University, Beijing 100084, China*

Received: 19 October 2013
Revised: 8 November 2013
Accepted: 12 November 2013

KEYWORDS
carbon nanotube sponge, polypyrrole, core–shell configuration, compressible electrode, supercapacitor

ABSTRACT

A carbon nanotube (CNT) sponge contains a three-dimensional conductive nanotube network, and can be used as a porous electrode for various energy devices. We present here a rational strategy to fabricate a unique CNT@polypyrrole (PPy) core–shell sponge, and demonstrate its application as a highly compressible supercapacitor electrode with high performance. A PPy layer with optimal thickness was coated uniformly on individual CNTs and inter-CNT contact points by electrochemical deposition and crosslinking of pyrrole monomers, resulting in a core–shell configuration. The PPy coating significantly improves specific capacitance of the CNT sponge to above 300 F/g, and simultaneously reinforces the porous structure to achieve better strength and fully elastic structural recovery after compression. The CNT@PPy sponge can sustain 1,000 compression cycles at a strain of 50% while maintaining a stable capacitance (> 90% of initial value). Our CNT@PPy core–shell sponges with a highly porous network structure may serve as compressible, robust electrodes for supercapacitors and many other energy devices.

1 Introduction

Three-dimensional networks or aerogels based on carbon nanotubes (CNTs) and graphene have shown wide applications such as porous electrodes, compressible foams for energy absorption, and environmental cleanup [1–4]. Recently, supercapacitors based on CNT films, aligned arrays, graphene aerogels and fibers have

Address correspondence to Anyuan Cao, anyuan@pku.edu.cn; Dehai Wu, wdh-dme@tsinghua.edu.cn

been studied extensively, with intensive efforts focused on performance improvement [5–10]. By tailoring the microstructure and appropriate functionalization of CNT and graphene-based electrodes, key parameters such as capacitance, energy and power densities have been enhanced continuously [11–15]. On the other hand, there has been limited progress in developing flexible supercapacitors that may extend applications to areas allowing the presence of stresses or material shape change. Examples of such applications include stretchable electrodes based on a buckled CNT film adhered to a plastic substrate [16, 17], and bendable or compressible electrodes based on solution-processed graphene aerogels [18–20]. Mechanical properties, which dominate the performance of flexible electrodes, have not been studied in-depth to date. In particular, structure robustness and elasticity during deformation need considerable improvement, and this demands the rational design and fabrication of CNT and graphene electrodes with optimized structure and properties.

Here, we present an effective approach to fabricate a porous CNT@polypyrrole (PPy) core–shell sponge based on a macroscopic CNT sponge reported by our team recently [21] and demonstrate the application of the hybrid sponge as highly compressible supercapacitor electrodes. Clean CNT sponges can work as a deformable electrode, but the specific capacitance produced by this double-layer capacitor is relatively low (28.5 F/g) [22]. Owing to the three-dimensional porous CNT network, we introduce a pseudomaterial, PPy, to wrap each nanotube and their contacts to simultaneously enhance the mechanical properties and supercapacitor performance. Previously, several conductive polymers have been electrochemically deposited onto CNTs (powders, films, and arrays) and graphene aerogels to improve specific capacitance, however, the morphology and distribution of polymers are difficult to control precisely [20, 23–26]. An important difference here is the CNT@PPy core–shell nanostructure. In addition, a uniform PPy coating throughout the sponge allows good control and optimization of the PPy layer thickness, a critical parameter for achieving high capacitance. Furthermore, structure reinforcement by such polymers, uniquely related to our isotropic, mutually contacted CNT network, has not been addressed before. In addition, the high elasticity of our PPy-coated sponges (sustaining many compression cycles without degradation) is superior to previous compressible CNT or graphene electrodes which typically can not recover elastically.

2 Experimental

2.1 Synthesis of CNT sponges

CNT sponge samples were synthesized by chemical vapor deposition (CVD). Ferrocene and 1,2-dichlorobenzene were used as the catalyst precursor and carbon source, respectively. A solution of ferrocene powder dissolved in dichlorobenzene at a concentration of 0.06 g/mL was continuously injected into the CVD furnace by a syringe pump at a constant feeding rate of 0.13 mL/min. A mixture of Ar (2,000 mL/min) and H_2 (300 mL/min) was used as carrier gas. The reaction temperature was 860 ℃. A quartz sheet was placed in the reaction zone to deposit and collect sponge samples. As-synthesized sponges were peeled off from the substrate.

2.2 Fabrication of CNT@PPy core–shell sponges

An as-grown bulk CNT sponge block with edge size of several mm was immersed in Py/acetone solution with a concentration in the range 0.1–1 M for 0.5 h. Then the CNT sponge with Py monomers adsorbed on the surface of each individual CNT was directly used as the working electrode under a potential of 0.8 V in 0.3 M $NaClO_4$ aqueous solution. The electropolymerization of Py was performed using a three-electrode electrochemical workstation (CHI660D Instruments, Shanghai, China). A Pt wire and Ag/AgCl were used as the counter and reference electrodes, respectively. A typical electropolymerization time was 5–10 min. After the electropolymerization process, the crosslinked CNT@PPy core–shell sponge was rinsed with distilled water and then freeze-dried to maintain the porous structure.

2.3 Material characterization

The sample morphology and structure were characterized using scanning electron microscopy (SEM) (LEO 1530) and transmission electron microscopy (TEM) (JEOL 2010). Raman spectra were recorded using a

RM 2000 Microscopic Confocal Raman Spectrometer (Renishaw PLC, England) with a 633 nm laser. Fourier transform infrared (FTIR) spectra were recorded on a FTIR system (Bruker Vector 22). X-ray photoelectron spectroscopy (XPS) measurements were performed using an ESCALAB 250Xi spectrometer. Thermogravimetric analysis (TGA) was conducted on a TGA Q5000 analyzer from 30 to 800 °C in air at a heating rate of 20 °C·min^{-1}. Mechanical tests were carried out by a single-column static instrument (Instron 5843) equipped with two flat-surface compression stages and a 10 N load cell. The N_2 adsorption and desorption isotherms were measured at 77 K in a liquid nitrogen bath using a QUANTACHROME Autosorb-iQ analyzer. The Brunauer–Emmett–Teller (BET) specific surface area of sponges was measured. The pore volume and pore size distribution were obtained using the Barrett–Joyner–Halenda (BJH) method.

2.4 Electrochemical measurements

Sponges were assembled into a prototype two-electrode symmetrical supercapacitor cell. Two blocks of CNT or CNT@PPy (with different loadings) sponges with a filter paper sandwiched in between were clamped by two polymeric blocks in the original state (no compression) or at predefined compressive strains (20%–50%). Platinum wires twisted around the polymeric clamps and connected to the sponge electrodes were used as current collectors. The electrochemical properties of the capacitor cell including cyclic voltammetry (CV), galvanostatic charge/discharge and electrochemical impedance spectroscopy (EIS) were measured using a CHI660D electrochemical workstation. The CV curves were measured with different scan rates from 2–200 mV/s between –0.45 and 0.45 V. EIS measurements were carried out in the frequency range from 100 kHz to 0.01 Hz at open circuit potential with an ac perturbation of 5 mV. Electrochemical measurements were carried out in a 2 M KCl aqueous electrolyte at room temperature. The specific capacitance of the supercapacitor cell (C_{Cell}) was calculated from the CV curves according to the following equation

$$C_{Cell} = \int \frac{I}{m} dV / v\Delta V$$

where I is the response current (A), m is the total mass of two sponge electrodes (including CNTs and PPy) (g), ΔV is the potential range (V), v is the potential scan rate (mV/s). The specific capacitance of the single electrode (C_s) was calculated by the equation $C_s = 4\ C_{Cell}$.

3 Results and discussion

Our strategy is to deposit a uniform layer of PPy within the CNT sponge, while maintaining the original network structure and high porosity, as illustrated in Fig. 1(a). To coat PPy around each individual CNT, we first immersed a block of sponge synthesized by chemical vapor deposition in our previous report [22] into a pyrrole (Py) solution to adsorb a layer of Py molecules on the nanotube surface which is hydrophobic in the as-synthesized state. Then, the Py monomers were crosslinked into a solid PPy layer by electropolymerization in a three-electrode cell with the sponge as the working electrode (see the Experimental section for details). The PPy loading (18–90 wt.%) relative to the CNT mass and the PPy layer thickness can be controlled by varying the Py concentration in acetone and the absorption period. In this way, we obtained a core–shell configuration in which each nanotube was wrapped (sheathed) by a uniform PPy layer. The resulting CNT@PPy sponge maintained a porous structure with a specific surface area (95 m^2/g) similar to the original sponge (80 m^2/g), with an increased percentage of pores with sizes in the range of 3–100 nm accessible by liquid electrolyte (see Fig. S1 in the Electronic Supplementary Material (ESM)). The main characteristics related to our core–shell sponges include (1) liquid electrolyte can infiltrate throughout the sponge to effectively utilize the internal PPy surface which provides necessary reactive sites, (2) charge carriers produced by the pseudoreaction on the PPy layer can arrive at the CNT across a minimal distance through the radial direction, and (3) the highly conductive CNT network embedded (and well preserved) under the PPy layer can transport charge carriers efficiently to external circuits. The above characteristics of our distinct core–shell configuration ensure an optimized and efficient charge transport and collection process, which is important for obtaining high capacitance. A bulk $1 \times 0.8 \times 0.6$ cm^3 CNT sponge

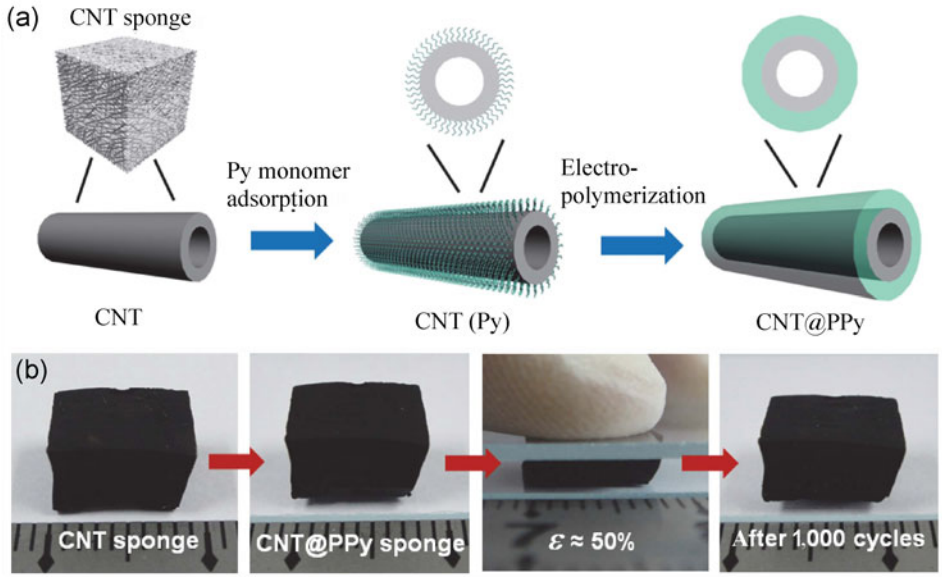

Figure 1 Illustration of the fabrication process from a CNT to a CNT@PPy core–shell sponge. (a) A layer of Py monomers was adsorbed on a CNT sponge and crosslinked into a uniform PPy coating on the surface of individual CNTs by electropolymerization. (b) Photos of a block of CNT sponge before and after PPy coating, and the CNT@PPy sponge under manual compression ($\varepsilon \approx 50\%$) and after 1,000 compression cycles (in the instrument).

maintains the same shape and size after PPy deposition, can be compressed to large strains without breaking or collapse, and recovers its original volume after many compression cycles (Fig. 1(b)).

SEM and TEM characterizations showed well-controlled PPy deposition and the resulting neat CNT@PPy core–shell sponge. Compared with the original sponge consisting of randomly overlapped CNTs, each nanotube has been wrapped by a PPy layer, and the average outer diameter has increased from about 44 nm (clean nanotubes) to 80 nm (with PPy) (Figs. 2(a) and 2(b)). The PPy layer thickness is about 18 nm corresponding to a loading of 52.4 wt.%, and can be adjusted in the range 5–60 nm by varying the loading (Fig. S2 in the ESM). Despite the thickening of the nanotubes, the sponge maintains a porous structure. The core–shell structure can be clearly observed in some regions where PPy has detached during SEM sample preparation, indicating the formation of a hybrid core–shell network (Fig. 2(c)). Because we first grafted Py monomers and then crosslinked them into a solid layer, the PPy coating is uniform throughout the sponge (both the internal part and the surface).

Interestingly, the contact points between adjacent nanotubes also have been coated by PPy, forming welded joints that are beneficial for structural stability and mechanical strength (Fig. 2(d)). Usually the welding of CNTs occurs at the points having mutual contact (or gaps narrower than the PPy thickness) in the original network. These inter-nanotube joints sustain the entire porous network, and prevent slippage of CNTs during movement. Therefore reinforcement of CNT contacts by PPy in the hybrid sponge is crucial to improve its deformability and elasticity. TEM images also show uniform CNT@PPy core–shell structures, and welding of two crossed nanotubes by a conformal PPy coating at their junction (Figs. 2(e) and 2(f)). Other characterization techniques including Raman spectroscopy, FTIR, XPS, and TGA all confirmed the successful crosslinking of PPy and its molecular structure (Fig. S3 in the ESM). In particular, TGA results show a higher weight loss temperature of the CNT@PPy (630 °C) compared to the uncoated sponge (590 °C), indicating strong adherence of PPy which could delay the combustion of CNTs inside (Fig. S3(d) in the ESM).

We carried out uniaxial compression tests on bulk CNT and core–shell sponges to study the effect of PPy coating on mechanical properties. Compressive stress–strain (σ–ε) curves clearly show the strengthening effect by PPy, with the maximum stress at $\varepsilon = 60\%$

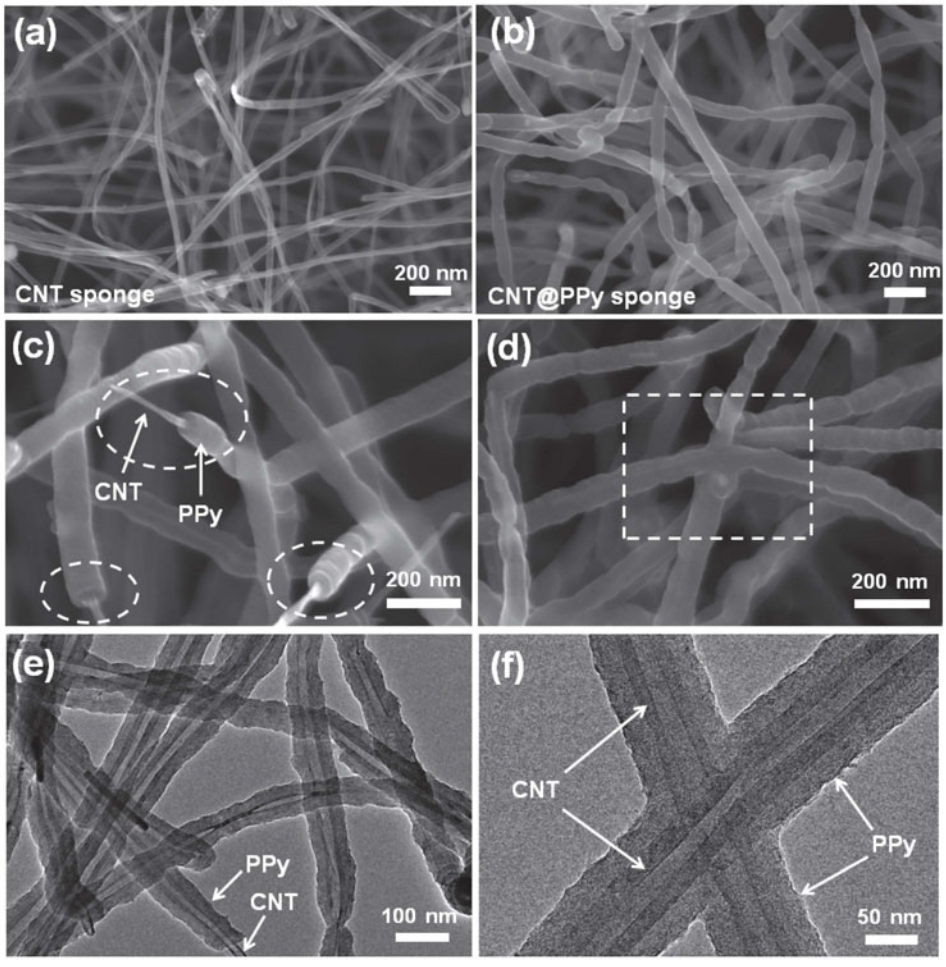

Figure 2 Structure characterization of CNT and core–shell sponges. (a) SEM image of the CNT sponge. (b) SEM image of the CNT@PPy (52.4 wt.%) sponge. (c) SEM image showing the core–shell structure of PPy-coated CNTs. (d) SEM image showing the PPy coating on inter-CNT contacts. (e) TEM image of CNT@PPy showing uniform core–shell structures. (f) High-magnification TEM image showing the PPy layer welding two crossed CNTs.

increasing from 44 (without PPy) to 110 kPa with 50.3 wt.% PPy (Fig. 3(a)). Higher loading results in thicker core–shell nanotubes, making the entire network more rigid and resistant to compression (but with a tendency to lose porosity). Furthermore, the dry CNT@PPy sponge (50.3 wt.%) exhibits elastic and full volume recovery after compression. For compressive strains up to 60%, the unloading curves all return to the origin without producing residual strain (or plastic deformation) and the compressed sample can rapidly expand back to its original shape (Fig. 3(b)). The CNT@PPy core–shell sponge with its hydrophilic surface can also be compressed in water and recover its original shape by water absorption (Fig. S4(a) in the ESM). Both CNT and hybrid sponges (with improved strength) can sustain repeated large-strain compression to $\varepsilon = 50\%$ for 1,000 cycles without stress degradation, indicating high structure stability (Fig. 3(c)). After 1,000 compression cycles, the CNT@PPy (50.3 wt.%) sponge develops a modest plastic deformation (residue $\varepsilon \approx 5\%$), which is smaller than the CNT sponge ($\varepsilon \approx 10\%$) and the CNT@PPy sponge with a lower loading of 28.7 wt.% ($\varepsilon \approx 7\%$) (Fig. 3(d) and Fig. S4(b) (in the ESM)). The enhanced elasticity and stability can be attributed to the PPy reinforcement of both nanotube segments and nanotube–nanotube contacts throughout the sponge. Previously reported compressible PPy–graphene foam electrodes only show elastic behavior in an aqueous environment or organic solvents (liquid absorption could drive volume recovery), not in the dry state [20].

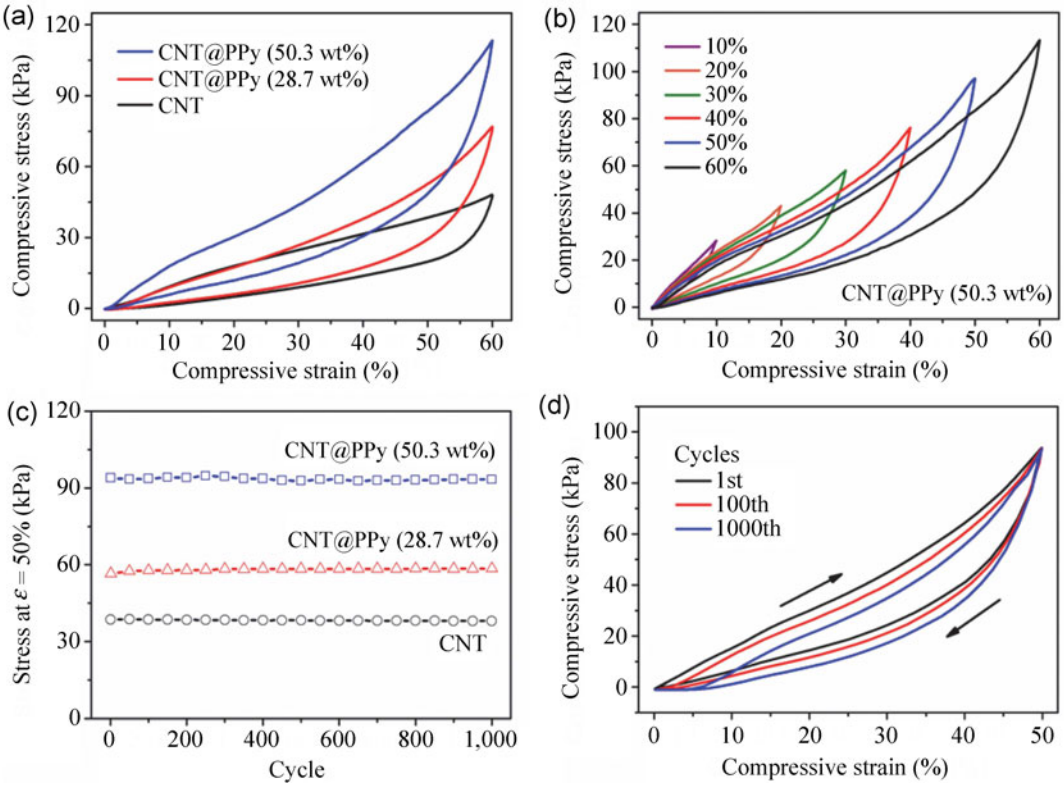

Figure 3 Mechanical properties of CNT and core–shell sponges. (a) Compressive stress–strain curves of a CNT and two CNT@PPy sponges with different PPy loadings at a set strain of 60%. (b) Stress–strain curves of a CNT@PPy (50.3 wt.%) sponge at different set strains from 10% to 60%. (c) Recorded stress values in the CNT and CNT@PPy sponges for 1,000 cycles at a set $\varepsilon = 50\%$. (d) Cyclic stress–strain curves of a CNT@PPy (50.3 wt.%) sponge at set $\varepsilon = 50\%$ including the first, 100th, and 1,000th cycles.

We assembled the elastic CNT@PPy sponges into a prototype two-electrode symmetrical supercapacitor in which *in situ* compression on the sponge could be performed by specially designed clamps (Fig. S5 in the ESM). CV tests were recorded in 2 M KCl aqueous electrolyte at different scanning rates. The PPy functionalization leads to significantly higher current density and an enlarged area enclosed by the charge/discharge curves, with a specific capacitance (at 200 mV/s) increasing from 10.1 F/g (for CNT sponge) to 255.4 F/g for the CNT@PPy sponge (52.4 wt.%) (Fig. 4(a)). The specific capacitance is calculated based on the total hybrid sponge weight, although the contribution from buried CNTs might be negligible compared to the PPy shell that is in direct contact with the electrolyte. This performance improvement can be attributed to the combined effect of a conformal PPy coating (responsible for pseudoreactions) supported by a three-dimensional CNT network (for efficient charge collection and transport). The highest capacitance is about 335 F/g obtained in the CNT@PPy sponge (52.4 wt.%) at a scan rate of 2 mV/s, compared with the CNT sponge (17 F/g) and the hybrid sponge with 18.2 wt.% PPy (249 F/g) and 80.9 wt.% (182 F/g) (Fig. 4(b)). This shows that further increasing the PPy loading in the sponge (to 80.9 wt.%) does not lead to a continued improvement in capacitance due to the increase in material weight and less efficient charge collection (through a thicker PPy layer) by CNTs. This further indicates that the significant improvement of the supercapacitor performance is due to the combination of the porous structure of CNT sponge and the high pseudocapacitance of PPy. Thus there exists an optimized PPy loading (~50 wt.%) with a layer thickness of ~20 nm which affords maximum capacitance. Figure 4(c) compares the galvanostatic charge–discharge curves of the CNT and CNT@PPy sponges measured at a constant current density of

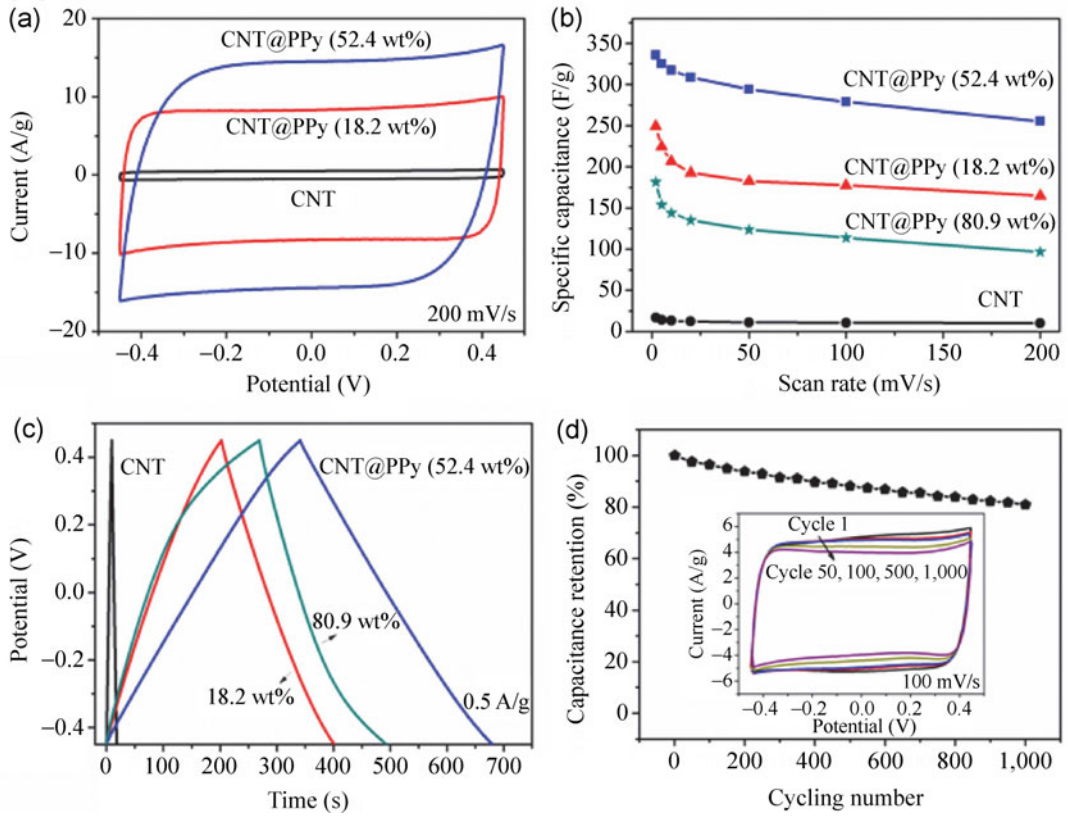

Figure 4 Supercapacitor application of CNT@PPy core–shell sponges. (a) CV curves of the CNT and CNT@PPy (18.2 wt.% and 52.4 wt.%) sponges at a scan rate of 200 mV/s. (b) Calculated specific capacitances of the CNT and CNT@PPy sponges with PPy loadings of 18.2 wt.%, 52.4 wt.%, and 80.9 wt.%,. (c) Galvanostatic charge/discharge curves of the CNT and CNT@PPy (18.2 wt.%, 52.4 wt.%, and 80.9 wt.%) sponges at a current of 0.5 A/g. (d) Cycling tests showing a capacitance retention of > 80% after 1,000 charge and discharge cycles at 100 mV/s. Inset shows CV curves of the 1st, 50th, 100th, 500th, and 1,000th cycles.

0.5 A/g. The highest specific capacitance calculated from the charge–discharge curves obtained in the CNT@PPy sponge (52.4 wt.%) is ca. 376 F/g, which is comparable to the results of the CV tests (335 F/g). The curves of the CNT@PPy sponges with PPy loadings of 18.2 wt.% and 52.4 wt.% are linear and symmetrical, while the curve symmetry decreases at higher loading (80.9 wt.%). This demonstrates that the CNT@PPy sponge possesses excellent electrochemical reversibility and charge–discharge properties with optimized PPy loading. In addition, the supercapacitor shows very low equivalent series resistance (ESR) as seen from the negligible voltage drop (IR drop). Cycling stability of the CNT@PPy electrode was investigated at a scan rate of 100 mV/s, and there was a certain degree of degradation in the current density and specific capacitance after 1,000 charge and discharge cycles (the capacitance drops to about 80% of initial value) (Fig. 4(d)). The CV cycling test and galvanostatic charge–discharge cycling test show comparable performance (Fig. S6(a)) and the EIS before and after 1,000 cycles remains stable (Fig. S6(b) in the ESM). We have further investigated the cycling stability for 5,000 cycles at a scan rate of 200 mV/s. The capacitance reached a stable level from the 4,000th cycle. After 5,000 charge and discharge cycles, it still maintained more than 60% of the initial specific capacitance (Figs. S6(c) and S6(d) in the ESM).

In addition to the improvement in specific capacitance resulting from PPy functionalization, the CNT@PPy sponges also show excellent performance under large compression. A CNT@PPy sponge (52.4 wt.%) supercapacitor exhibits similar CV curves at compressive strains of ε = 20% and 50% compared with the original (un-compressed) state (Fig. 5(a)). Under compression, the charge and discharge current

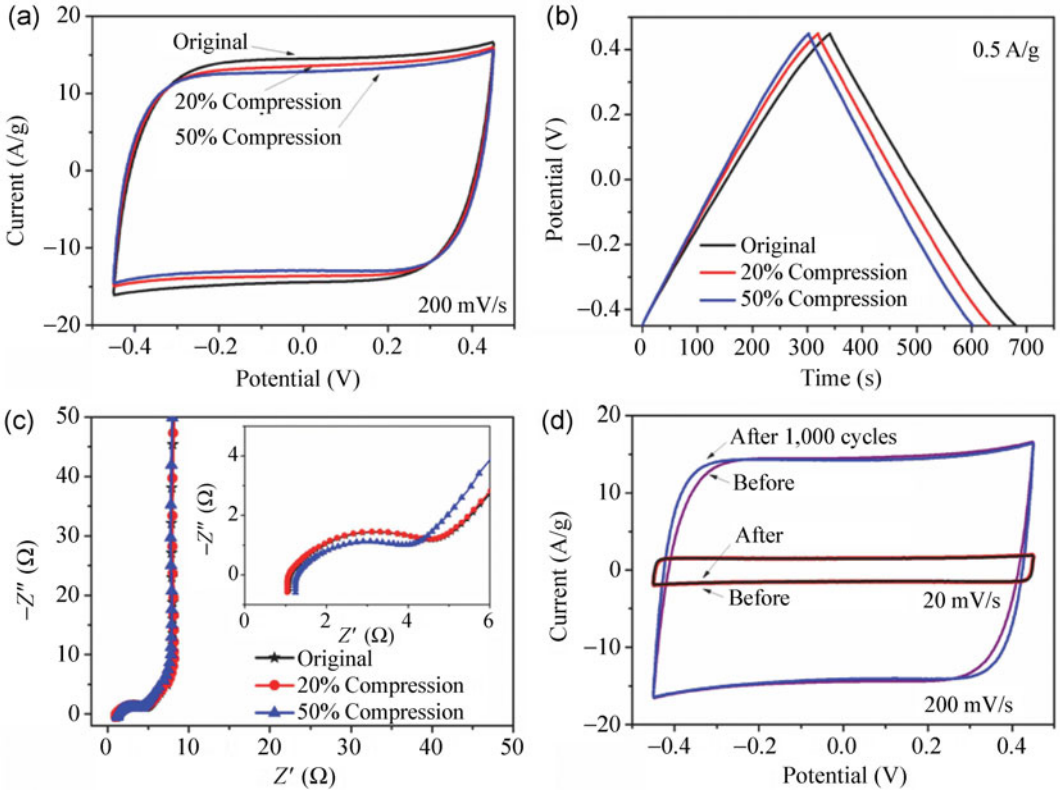

Figure 5 Supercapacitor performance of CNT@PPy core–shell sponges under compression. (a) CV curves of a CNT@PPy (52.4 wt.%) sponge in the original and compressed states (ε = 20% and 50%) at 200 mV/s. (b) Corresponding galvanostatic charge/discharge curves of the CNT@PPy (52.4 wt.%) sponge in the original and compressed states at a current of 0.5 A/g. (c) Electrochemical impedance spectroscopy of the CNT@PPy (52.4 wt.%) sponge in the original and compressed states. Inset is the magnification of Warburg semicircles from the spectra. (d) CV cures of a CNT@PPy sponge before and after 1,000 compression cycles (ε = 50%) tested at 200 and 20 mV/s.

densities decreased by < 7%, and the highly deformed sponge electrode still retained more than 90% of the original specific capacitance. Even with significant volume reduction, the three-dimensional core–shell nanotube network can maintain an open porous structure to allow electrolyte infiltration, which is important for ion diffusion and minimizing capacity loss. Figure 5(b) shows the galvanostatic charge–discharge curves of the CNT@PPy sponge (52.4 wt.%) in the original and compressed states. Even under a high compressive strain (50%), the charge–discharge curve of the CNT@PPy sponge maintains a linear and symmetrical shape. The EIS of the CNT@PPy sponge (with 52.4 wt.% PPy) is shown in Fig. 5(c). The Nyquist plots consist of a typical semicircle in the high frequency region and a straight line at low frequency. The CNT@PPy sponge shows similar Nyquist plots in original and compressed states (ε = 20% and 50%), indicating a stable ESR (1.08–1.24 Ω) under compression. We further investigated the supercapacitor performance of the CNT@PPy sponge under cyclic compression. After 1,000 compression cycles to a set strain of ε = 50%, the CNT@PPy sponge shows similar specific capacitance (304 and 264 F/g) to that of the original sponge (310 and 268 F/g) at 20 and 200 mV/s, respectively (Fig. 5(d)). The CV curves at low scan rate (20 mV/s) are nearly identical before and after cyclic compression. The elastic sponge might be able to sustain many more compression cycles (at modest to moderate strains) without appreciable structure and performance degradation. This result indicates that the CNT@PPy sponge can work as a robust electrode with stable capacitor behavior under cyclic compression conditions.

4 Conclusion

We have demonstrated the rational design and fabrication of CNT@PPy core–shell sponges with high structural elasticity and stable supercapacitor performance under repeated compression cycles. We found that an appropriate PPy loading and layer thickness are important factors for simultaneous structure reinforcement and significant improvement in specific capacitance. The CNT sponges provide a general platform on which functional materials can be introduced in controlled way to enable multifunctionality and extend areas of application. CNT@PPy core–shell sponges with a highly porous network structure may serve as compressible, robust electrodes for supercapacitors and many other energy devices.

Acknowledgements

This work was supported by the National Natural Science Foundation of China (NSFC, No. 91127004) and the Beijing City Science and Technology Program (No. Z121100001312005).

Electronic Supplementary Material: Supplementary material (nitrogen sorption isotherms and pore size distribution of CNT and CNT@PPy sponges, TEM images of PPy-coated CNTs in the CNT@PPy sponges, characterization of the CNT and CNT@PPy sponges by Raman, FTIR, XPS, and TGA, plastic deformation of CNT and CNT@PPy sponges, CV curves of a supercapacitor cell containing two CNT@PPy sponge electrodes, and cycling stability tests) is available in the online version of this article at http://dx.doi.org/10.1007/s12274-013-0388-5.

References

[1] Bordjiba, T.; Mohamedi, M.; Dao, L. H. New class of carbon-nanotube aerogel electrodes for electrochemical power sources. *Adv. Mater.* **2008**, *20*, 815–819.

[2] Zhang, X. T.; Sui, Z. Y.; Xu, B.; Yue, S. F.; Luo, Y. J.; Zhan, W. C.; Liu, B. Mechanically strong and highly conductive graphene aerogel and its use as electrodes for electrochemical power sources. *J. Mater. Chem.* **2011**, *21*, 6494–6497.

[3] Kim, K. H.; Oh, Y.; Islam, M. F. Graphene coating makes carbon nanotube aerogels superelastic and resistant to fatigue. *Nat. Nanotechnol.* **2012**, *7*, 562–566.

[4] Li, H. B.; Gui, X. C.; Zhang, L. H.; Ji, C. Y.; Zhang, Y. C.; Sun, P. Z.; Wei, J. Q.; Wang, K. L.; Zhu, H. W.; Wu, D. H., et al. Enhanced transport of nanoparticles across a porous nanotube sponge. *Adv. Funct. Mater.* **2011**, *21*, 3439–3445.

[5] Izadi-Najafabadi, A.; Yasuda, S.; Kobashi, K.; Yamada, T.; Futaba, D. N.; Hatori, H.; Yumura, M.; Iijima, S.; Hata, K. Extracting the full potential of single-walled carbon nanotubes as durable supercapacitor electrodes operable at 4 V with high power and energy density. *Adv. Mater.* **2010**, *22*, E235–E241.

[6] Futaba, D. N.; Hata, K.; Yamada, T.; Hiraoka, T.; Hayamizu, Y.; Kakudate, Y.; Tanaike, O.; Hatori, H.; Yumura, M.; Iijima, S. Shape-engineerable and highly densely packed single-walled carbon nanotubes and their application as super-capacitor electrodes. *Nat. Mater.* **2006**, *5*, 987–994.

[7] He, Y. M.; Chen, W. J.; Li, X. D.; Zhang, Z. X.; Fu, J. C.; Zhao, C. H.; Xie, E. Q. Freestanding three-dimensional graphene/MnO_2 composite networks as ultralight and flexible supercapacitor electrodes. *ACS Nano* **2013**, *7*, 174–182.

[8] Choi, B. G.; Yang, M. H.; Hong, W. H.; Choi, J. W.; Huh, Y. S. 3D macroporous graphene frameworks for supercapacitors with high energy and power densities. *ACS Nano* **2012**, *6*, 4020–4028.

[9] Li, X. M.; Zhao, T. S.; Wang, K. L.; Yang, Y.; Wei, J. Q.; Kang, F. Y.; Wu, D. H.; Zhu, H. W. Directly drawing self-assembled, porous, and monolithic graphene fiber from chemical vapor deposition grown graphene film and its electrochemical properties. *Langmuir* **2011**, *27*, 12164–12171.

[10] Meng, Y. N.; Zhao, Y.; Hu, C. G.; Cheng, H. H.; Hu, Y.; Zhang, Z. P.; Shi, G. Q.; Qu, L. T. All-graphene core-sheath microfibers for all-solid-state, stretchable fibriform supercapacitors and wearable electronic textiles. *Adv. Mater.* **2013**, *25*, 2326–2331.

[11] Qian, X. F.; Lv, Y. Y.; Li, W.; Xia, Y. Y.; Zhao, D. Y. Multiwall carbon nanotube@mesoporous carbon with core–shell configuration: A well-designed composite-structure toward electrochemical capacitor application. *J. Mater. Chem.* **2011**, *21*, 13025–13031.

[12] Jha, N.; Ramesh, P.; Bekyarova, E.; Itkis, M. E.; Haddon, R. C. High energy density supercapacitor based on a hybrid carbon nanotube-reduced graphite oxide architecture. *Adv. Energy Mater.* **2012**, *2*, 438–444.

[13] Liu, C. G.; Yu, Z. N.; Neff, D.; Zhamu, A.; Jang, B. Z. Graphene-based supercapacitor with an ultrahigh energy density. *Nano Lett.* **2010**, *10*, 4863–4868.

[14] Yu, G. H.; Hu, L. B.; Liu, N.; Wang, H. L.; Vosgueritchian, M.;

Yang, Y.; Cui, Y.; Bao, Z. N. Enhancing the supercapacitor performance of graphene/MnO_2 nanostructured electrodes by conductive wrapping. *Nano Lett.* **2011**, *11*, 4438–4442.

[15] Kim, T. Y.; Lee, H. W.; Stoller, M.; Dreyer, D. R.; Bielawski, C. W.; Ruoff, R. S.; Suh, K. S. High-performance supercapacitors based on poly(ionic liquid)-modified graphene electrodes. *ACS Nano* **2011**, *5*, 436–442.

[16] Yu, C. J.; Masarapu, C.; Rong, J. P.; Wei, B. Q.; Jiang, H. Q. Stretchable supercapacitors based on buckled single-walled carbon-nanotube macrofilms. *Adv. Mater.* **2009**, *21*, 4793–4797.

[17] Niu, Z. Q.; Dong, H. B.; Zhu, B. W.; Li, J. Z.; Hng, H. H.; Zhou, W. Y.; Chen, X. D.; Xie, S. S. Highly stretchable, integrated supercapacitors based on single-walled carbon nanotube films with continuous reticulate architecture. *Adv. Mater.* **2013**, *25*, 1058–1064.

[18] El-Kady, M. F.; Strong, V.; Dubin, S.; Kaner, R. B. Laser scribing of high-performance and flexible graphene-based electrochemical capacitors. *Science* **2012**, *335*, 1326–1330.

[19] Xu, Y. X.; Lin, Z. Y.; Huang, X. Q.; Liu, Y.; Huang, Y.; Duan, X. F. Flexible solid-state supercapacitors based on three-dimensional graphene hydrogel films. *ACS Nano* **2013**, *7*, 4042–4049.

[20] Zhao, Y.; Liu, J.; Hu, Y.; Cheng, H. H.; Hu, C. G.; Jiang, C. C.; Jiang, L.; Cao, A. Y.; Qu, L. T. Highly compression-tolerant supercapacitor based on polypyrrole-mediated graphene foam electrodes. *Adv. Mater.* **2013**, *25*, 591–595.

[21] Gui, X. C.; Wei, J. Q.; Wang, K. L.; Cao, A. Y.; Zhu, H. W.; Jia, Y.; Shu, Q. K.; Wu, D. H. Carbon nanotube sponges. *Adv. Mater.* **2010**, *22*, 617–621.

[22] Li, P. X.; Kong, C. Y.; Shang, Y. Y.; Shi, E. Z.; Yu, Y. T.; Qian, W. Z.; Wei, F.; Wei, J. Q.; Wang, K. L.; Zhu, H. W., et al. Highly deformation-tolerant carbon nanotube sponges as supercapacitor electrodes. *Nanoscale* **2013**, *5*, 8472–8479.

[23] Feng, W.; Bai, X. D.; Lian, Y. Q.; Liang, J.; Wang, X. G.; Yoshino, K. Well-aligned polyaniline/carbon-nanotube composite films grown by *in-situ* aniline polymerization. *Carbon* **2003**, *41*, 1551–1557.

[24] Lota, K.; Khomenko, V.; Frackowiak, E. Capacitance properties of poly(3,4-ethylenedioxythiophene)/carbon nanotubes composites. *J. Phys. Chem. Solids* **2004**, *65*, 295–301.

[25] Hu, Y.; Zhao, Y.; Li, Y.; Li, H.; Shao, H. B.; Qu, L. T. Defective super-long carbon nanotubes and polypyrrole composite for high-performance supercapacitor electrodes. *Electrochimi. Acta* **2012**, *66*, 279–286.

[26] Cong, H. P.; Ren, X. C.; Wang, P.; Yu, S. H. Flexible graphene-polyaniline composite paper for high-performance supercapacitor. *Energy Environ. Sci.* **2013**, *6*, 1185–1191.